Implementation of Data-Driven Approaches for Condition Assessment of Structures and Analyzing Complex Data

1 Introduction

Both concrete and steel structures are exposed to internal and external degradation and damaging agents during their service life. For example, concrete structures are susceptible to alkali-silica reaction, rebar corrosion, salt crystallization, sulfate attack, freeze and thaw cycles, delayed ettringite formation, etc. These types of degradation and damage endanger the durability and serviceability of structures. Cracks are formed due to the agents mentioned above, and extension and coalescence of existing cracks will inevitably impair the integrity of concrete structures. Steel structures are also exposed to corrosion and brittle cracking. Reconstructing damaged infrastructure is very expensive and requires a large amount of resources and energy. Therefore, structural inspection and monitoring have become more significant in recent years. Structural health monitoring of essential infrastructure can lead to a reasonable extension of structural service life.

Acoustic emission (AE) is one method for structural health monitoring. AE is a phenomenon wherein a material emits stress waves due to a sudden release of energy, such as cracking (ASTM, 2006). Piezoelectric sensors are used to acquire these mechanical waves and transfer them to digital signals. The signals have valuable information about the crack formation and the internal condition of materials in which cracks are formed. Many studies have focused on the use of AE to localize crack formation, assess damage, and monitor structural health (ElBatanouny, et al., 2014, Lokajíček, et al., 2017, Shiotani, 1994, Shiotani, et al., 2017, Soltangharaei, et al., 2021a, Soltangharaei, et al., 2019b).

Acoustic emission data typically includes parametric features extracted from the signals. Managing, analyzing, understanding, and interpreting data may be challenging due to the complexity of the data attributed to structural detailing, the duration of monitoring, and the temporal evolution of the acoustic property of the material. Today, several data-driven methods are available to overcome challenges attributed to data and the prediction of data patterns, including methods based on statistical concepts and machine learning algorithms.

2 AE wave sources in different structures

AE waves are emitted due to different mechanisms in structures. In the following section, some degradation mechanisms leading to AE wave generation are discussed.

2.1 Stress corrosion cracking

Cracks may be initiated and propagated in steel structures under corrosive conditions. Cracking in a steel structure is referred to as stress corrosion cracking (SCC) when it is caused by applying stress under corrosive conditions. Steel alloys used in structures are commonly considered to be ductile or flexible in nature. When steel alloys are exposed to high temperatures, they can become sensitive to corrosion. The corrosion products formed in the steel are more brittle than the original ductile steel and vulnerable to cracking. Therefore, in the presence of stress cracking may initiate. This degradation process can also be observed in austenitic stainless-steel alloys when the steel chemical species are altered due to exposure to high temperatures (e.g. welding). The carbon in the material bonds with the chromium and forms carbides in the grain boundaries, which reduces the concentration of chromium near the grain boundaries and makes the steel more susceptible to intergranular SCC (Soltangharaei, et al., 2020c). The following figure shows how the heat treatment affects the crystal structure of 304 L stainless steel.

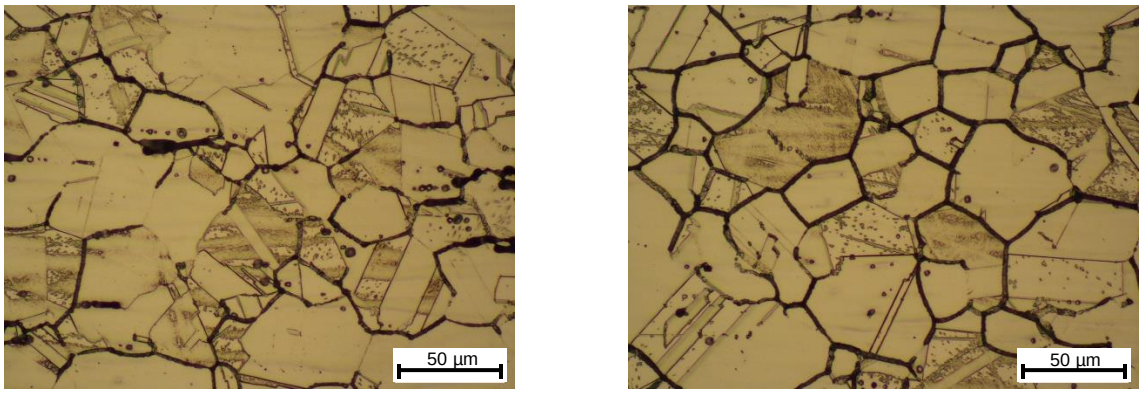

(a) Sensitization after 2 hours (b) Sensitization after 14 hours

Figure 1 Evolution of crystal structure of steel during heat treatment (Soltangharaei, et al., 2020c)

One potential risk of SCC in the structure is related to dry cask storage systems (DCSS). DCSSs are a temporary nuclear waste disposal system which has been utilized since the 1970s. The structures are stainless-steel canisters (vertical cylinders) which encase used nuclear fuel and high-level waste. The DCSSs are covered by a steel lid, which is welded to the canister. The welding on the storage containers causes austenitic materials

to become sensitized and more susceptible to SCC. Microcracks are expected to form at the welded region due to the exposure of DCSSs to the environment. Microcracks will widen, extend, and become macro-cracks. The cracking endangers the serviceability of DCSSs and may eventually lead to concerns with radiation leakage to the environment.

Visually inspecting the cracks in the steel canisters is challenging. Furthermore, these storage structures are usually under restricted access, which prohibits inspections on a regular-basis. AE technology can be employed in this case, taking advantage of the high sensitivity of the AE sensors as well as the non-destructive nature of the method. Microcracks are initiated at the welded region of the canisters. Then, stress waves are generated and travel through the material to reach an AE sensor. Minimal numbers of sensors may be attached at the bottom of the canister or on the base.

2.2 Cracking due to alkali-silica reaction

Many concrete structures such as dams, bridges, nuclear structures, and hydraulic structures are exposed to alkali-silica reaction (ASR). ASR is a chemical reaction which occurs between alkali hydroxides and siliceous minerals in some aggregates used in concrete structures (Rajabipour, et al., 2015, Villeneuve, et al., 2012). Reaction components are available in concrete structures. The reaction product is a hygroscopic gel, which is formed around and/or inside aggregates (Bažant and Steffens, 2000, Dron and Brivot, 1992, Hanson, 1944, Jun and Jin, 2010, Ponce and Batic, 2006). This gel tends to absorb moisture from concrete pores or premature cracks and then expands. The volume of the gel is larger than the original components of the reaction. Therefore, the gel exerts pressure on the surrounding concrete components, such as aggregates, cement paste, and interfacial transition zones. If the gel finds a way (cracks or void) to flow, its pressure will drop, otherwise, the pressure will accumulate and surpass the material fracture strength causing microcracks and crack extensions in the concrete. ASR in a concrete structure can be accompanied by other degradation agents such as freeze and thaw cycles, chloride penetration in concrete and steel corrosion, and delayed ettringite formation, which expedites degradation.

The reaction rate depends on several factors such as reactivity of aggregates, the Sodium and Potassium ion content in the cement, the availability of alkali-hydroxides in the pore solution, high humidity (more than 80%), high temperature (Saouma and Hariri-Ardebili, 2014), and confinement from different directions (Allard, et al., 2018, Barbosa, et al., 2018, Karthik, et al., 2016).

The ASR microcracks inside a concrete structure merge and widen through the ASR process. The reaction starts with a lower rate, then the rate increases followed by a decrease (Saouma and Perotti, 2006). The ASR progress rate can be observed by measuring the expansion of concrete. The expansion strain has a trend similar to the reaction. The following figure shows the volumetric strain of concrete blocks exposed to high temperature and humidity for 560 days (Figure 2a).

Another important factor in cracking due to ASR is internal or external confinement. Concrete structures can be internally confined against a specific direction due to existing reinforcements perpendicular to that direction. Furthermore, the confinement may be externally imposed on a structure. One example is a rigid structure, which may restrain an adjacent structure from ASR expansion in a specific direction. Confinement in one direction does not necessarily prevent the concrete from cracking. According to Figure 2b, the confined concrete block was cracked mostly in one direction, while cracking in the unconfined block was more randomly distributed (Figure 2c). The direction of the crack opening in the confined specimen is perpendicular to the plane with reinforcements as shown in Figure 2b.

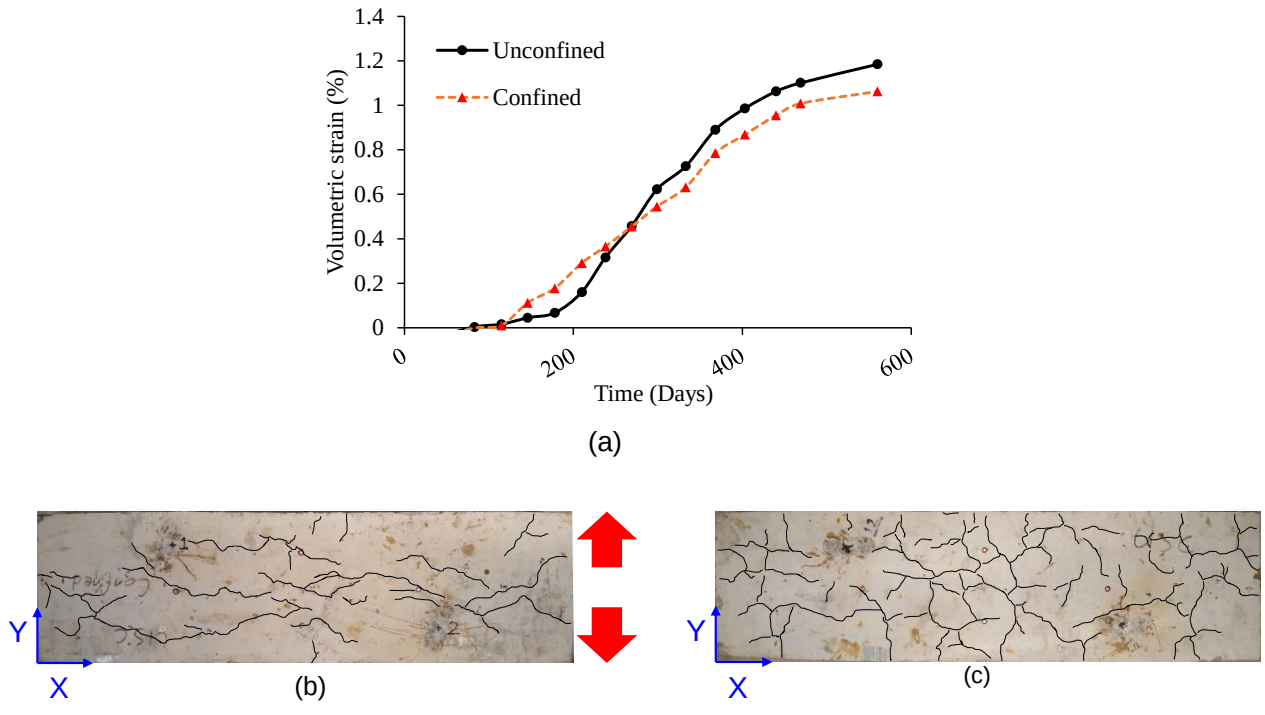

Figure 2 (a) Volumetric strain of concrete blocks due to accelerated ASR; (b) cracking on confined specimen; (c) cracking on unconfined specimen.

Stress waves are generated due to ASR crack formation in a concrete structure and are recorded as digital signals. Signal features may be affected by the fracture mechanism of active cracking in different ASR stages, the potential evolution of internal acoustic properties of concrete during ASR, sensor coupling, structure geometry, and concrete components (rebars, aggregate size and type, void ratio).

2.3 Loading and impact

AE signals can be generated by the crack formation induced by external loading or impacts. In terms of material science, AE can be used to investigate the different cracking mechanisms and fracture mechanics. The crack mechanisms can be identified by moment tensor analysis (Ohtsu, 1995) or using machine learning methods (Anay, et al., 2018, Soltangharaei, et al., 2021b). Furthermore, more detailed information is obtained about the failure mechanism of structural components using AE during a full-scale test (Abdelrahman, et al., 2014).

Load testing is also used as a procedure to evaluate the condition of structures under service loads. In the United States, load tests are conducted using standard truck loads to assess the condition of bridges and remove the load postings. One method to evaluate the superstructural components of a bridge is to calculate displacement distribution factors between the slabs using displacement and strain sensors during load tests. However, using conventional load testing is time-consuming and costly.

Concrete superstructural components of bridges (bridge decks or girders) have cracks and defects due to premature concrete conditions or degradation factors. Existing cracks in bridge decks or girders open or extend as a truck passes over the bridge, generating stress waves. These waves can be captured by AE sensors placed on bridge components. The advantage of AE over stain gauges or displacement sensors is its higher sensitivity, which can be helpful for bridge evaluation (Anay, et al., 2020).

AE monitoring is not limited to civil engineering infrastructure, but can also be utilized in aerospace structures. AE waves are generated by the impact of debris or hail striking an airplane component, such as an elevator, during flight. The impacts might cause minor damage, referred to as barely visible impact damage (BVID), on a surface manufactured with fiber composite material (Soltangharaei, et al., 2019b). The location and level of damage is correlated with the evolution of AE signal features. The following figure illustrates impacting on an airplane elevator used to collect AE data for a machine learning algorithm.

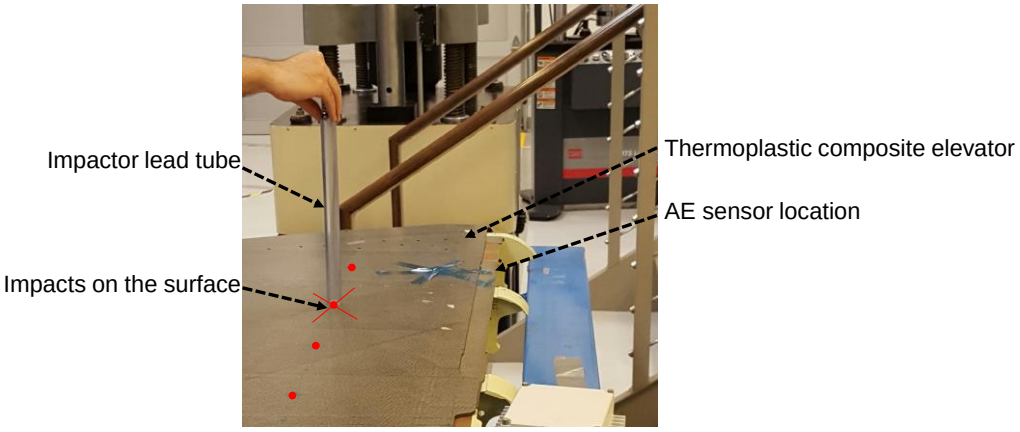

Figure 3 Impacting an airplane elevator for data collection (Soltangharaei, et al., 2019a).

3 Data analysis approaches

Data-driven techniques aim to find inherent features and structures of complex phenomena by evaluating data from different aspects (Hayashi, 1998). Data-driven techniques are based on mathematical relationships, which are derived from experimental data (Solomatine, et al., 2009) and can be used for damage detection and prediction when a physical model is not available, but the historical damage behavior is accessible. Although the data-driven methods are efficient for a noisy dataset and complex behavior, they may also be computationally expensive. However, the former drawback is diminishing due to progressive advances in computational hardware and cluster computers.

In physics-based methods, the availability of a physical model and loading conditions are essential. Each model should be validated and its parameters determined before application, which is not always feasible and straightforward (An, et al., 2015). Computational intelligence, machine learning, and regression are three examples of data-driven methods (Solomatine, et al., 2009). Pattern recognition can be categorized under the machine learning field, which focuses on discovering the regularities inside a data set by employing computer algorithms. There are two main categories associated with this method: unsupervised and supervised pattern recognition. Unsupervised pattern recognition is utilized to find and cluster unlabeled data when no predefined pattern is available. On the other hand, supervised pattern recognition is employed when a large labeled dataset is accessible for training. Subsequently, the trained algorithm can be engaged to classify new data (Bishop, 2006).

3.1 Data preparation before analysis

Although the high sensitivity of AE is employed for early detection of deterioration or damage, this advantage might lead to collecting a large amount of data during acquisition, which brings more challenges to data management and analysis. Therefore, different approaches should be taken to recognize more valuable data (essential data) within the raw data. Extraneous AE data may be collected for several reasons in a data acquisition system. Background noise, electrical noise, mechanical noise, boundary reflection data, and irrelevant environmental data are among the non-genuine data which may potentially be recorded during structural monitoring. Background noise is usually handled by setting an appropriate threshold in a system before running a test. The first step before using an AE system is to run a background noise test for a few hours to make sure the test environment is not acoustically contaminated. Using this information, an appropriate amplitude threshold for the system can be set. Furthermore, it is recommended that an AE sensor be attached to a component in a control condition during the test. Mechanical noise may be generated by friction between the structural components during loading of the structures or between the structure and the loading instruments. The solution for reducing the mechanical noise is isolating the loading instrumentation as much as possible from the structure by using materials with minimal acoustic impedance, such as neoprene pads, and/or a guard sensor near components with a friction potential.

Electrical noise usually appears in electrical components such as connections, cables, channels, or faulty sensors. Water penetration in connections is also one reason for electrical noise that may occur during long-term monitoring of structures exposed to environmental precipitation or high-humidity conditions. Fortunately, electrical noise can be clearly recognized from genuine data sets (Figure 4). Electrical noise has a low average frequency and peak frequency and can be removed by applying frequency-based filters. The hit rates for electrical noise are high, which may cause acquisition and buffering issues. Therefore, it is recommended to check electrical components and protect them from water by utilizing shrinkage tubes.

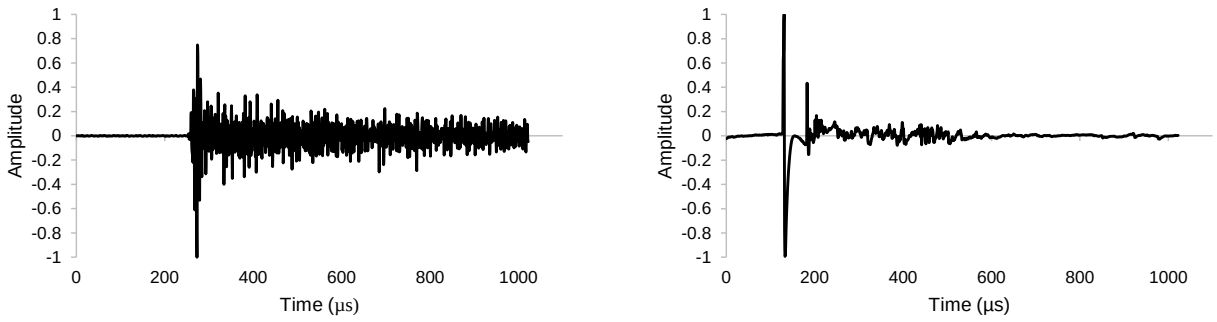

(a) (b)

Figure 4 Comparison between (a) genuine AE data; and (b) electrical connection noise.

Stress waves are reflected when they reach a media with different impedance or structure boundaries. In small-scale specimen tests receiving a large amount of reflections can be confusing in terms of data processing. A simple method to filter the reflections is using front-end filters (Ziehl and ElBatanouny, 2015). This is usually set in a data acquisition system by defining timing setups such as hit definition time (HDT), peak definition time (PDT), and hit lockout time (HLT) (MISTRASGroup, 2011). HLT is a parameter which is directly associated with removing a signal tailing or reflections. It refers to a time at the end of a signal where any threshold crossing is neglected. The amount of tailing data after an event can be adjusted using HLT.

AE raw data should go through several filters to be useful for data analysis and damage assessment procedures. One of the most traditional filtering methods is the Swansong II filter (Fowler, et al., 1989, Soltangharaei, et al., 2018). In this method, distributions of log (duration) versus amplitude (in decibels (dbAE)) or log (rise time) versus amplitude (in dbAE) are used to determine non-genuine data. Genuine AE data with low-amplitude generally has low-duration, and data with high-amplitude generally has high-duration. The other data, which does not follow the stated rule, is referred to as non-genuine data and is deleted. In this method, filtering limits are determined by observing the AE waveforms one by one in different amplitude intervals. Therefore, this is therefore time-consuming and not consistent. The latter disadvantage means that the filtering method depends on experience and preferences, i.e., the data filtered by two people may be different. Therefore, research has been conducted using statistical and signal processing methods for data filtering (Abdelrahman, et al., 2019, Sagasta, et al., 2014, Sagasta, et al., 2013). Abdelrahman, et al. (2019) employed the continuous wavelet transform to recognize genuine data from noisy data. Despite using different methods for filtering,

accuracy and performance in different applications is still under question and it appears that the Swansong II filter remains one of the most reliable methods for AE filtering. However, as mentioned, this method is time-consuming and challenging for long-term monitoring and low-level AE, where acquired data might be as large as a hundred gigabytes or a few terabytes. For this case, attaching several sensors on a structure in the sensitivity distance range of sensors can be beneficial for fast filtering. As an example, a script has been developed to filter AE data based on event definition (Soltangharaei, et al., 2020a, Soltangharaei, et al., 2020c). In the code, the hits registered by a specific number of sensors in specific time differences are recognized and retained as a genuine data set. The number of sensors depends on the number of sensors used in the test and the source location scope of project. Two-dimensional planes and three-dimensional spaces require at least three and four sensors, respectively, for source localization using triangulation. This filtering method has been found to be faster and more consistent than traditional methods. The algorithm is applicable to both parametric data and waveforms.

In the end, the pre-mentioned filtering methods are efficient to some extent but none may filter all extraneous data; hence random visual inspection of filtered data is recommended to check the efficiency of the filtering method and remove remaining potential non-geniune data.

After filtering, AE data should be organized and prepared for analyzing purposes. For example, the time attributed to data is modified to represent real-time monitoring, and the data is usually organized by the time.

3.2 Statistical analysis and distributions

AE waveforms are non-stationary signals (Suzuki, et al., 1996a). Therefore, different statistical and signal processing methods can be used to analyze data and derive essential information from the complex data. The outliers in signal features can be identified using statistical methods. In statistics, an outlier is defined as an observation with a large deviation from other observations (Hawkins, 1980). Outliers in a dataset may result in confusion and errors in some data-driven techniques. For instance, k-means methods are expected to misclassify a dataset with outliers (Tan, et al., 2013). Therefore, in some data-driven techniques, identification and removing outliers from data before conducting any analyses is significant. One of the simplest statistical methods is end-trimming data. In this method, a percentage (i.e., 5% or 10%) of the highest and lowest data is considered as outlier data and removed from the data set (Ott and Longnecker, 2015). Another common statistical method is using box-and-whiskers plots. By calculating a median, lower quartile, and upper quartile, a boxplot can be

drawn for a dataset. Then an inner fence and an outer fence are determined using quartiles and an interquartile range. Finally, mild and extreme outliers are identified by observing the data in the inner and outer fences (Ott and Longnecker, 2015).

Deriving a statistical distribution from AE data can be helpful for AE feature analyses. For example, distribution events along a specific dimension can be representative of cracking distribution (Soltangharaei, et al., 2020a). In Figure 5, event medians, first, and third quartiles are shown. The median line separates the lowest 50% and highest 50% of data, and the first and third quartiles split the lowest 25% of the data from the highest 75%, and the highest 25% of data from the lowest 75%, respectively. The vertical axis of the figure is the relative frequency of events. For example, in Figure 5a, the value for the first bin from the left is approximately equal to 0.04, which means only 4% of data is between 0 to 1.6 cm. In other words, the probability of event occurrence between 0 to 1.6 cm is 4%. The distribution for the confined specimen is completely different from the unconfined specimen.

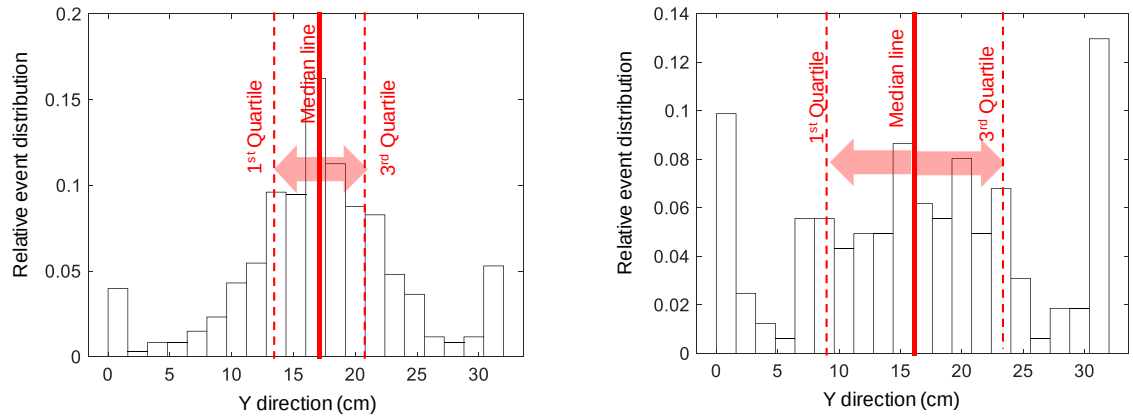

Figure 5 Relative event distribution for concrete specimens exposed to ASR deterioration, (a) Confined specimen; (b) unconfined specimens (Soltangharaei, et al., 2020a).

Another application of statistical methods is using a relative frequency histogram of signals to calculate Shannon entropy, which is explained in the next section.

The Gutenberg-Richter equation is the basis for b-value analysis (Rao and Lakshmi 2005), which is used in seismology and risk analysis to determine the realtionship between the frequency of an event occuranace and the event magnitude. The modified version of this method has been used for AE data as a damage index (Colombo, et al., 2003, Jung, et al., 2017, Rao and Lakshmi, 2005, Shiotani, 1994). The relationship between

AE amplitude (in dBAE) and the number of AE signals with amplitudes larger than A (signal amplitude) is presented as follows:

$$LogN = a - b(\frac{A}{20}) \quad (1)$$

Linear regression can be used to estimate *a* and *b* because the relationship between *logN* and *A* is close to linear. Two approaches are recommended to calculated b-values, incremental b-value and global b-value (Soltangharaei, et al., 2020c). In the former method, the entire data is separated according to intervals and b-values are calculated for the data in each interval. In the global b-value, b-values are calculated for each time, by considering the AE data that occurred before that time.

In addition to b-values, the coefficient of determination (R^2-value) can be calculated to identify the deviation of data from the linear relationship (Soltangharaei, et al., 2020c). The parameter can be used as a damage identification criterion. AE signals are emitted with a higher rate and larger energy or amplitude when severe damage or cracking occurs in a structure. AE signals with higher amplitude cause AE data to deviate from the b-value relationship decreasing the coefficient of determination for the system. R^2-value is calculated from the following equation:

$$R^2 = 1 - \frac{\sum_{i=1}^{n}(\hat{y}_i - y_i)^2}{\sum_{i=1}^{n}(y_i - \bar{y})^2} \quad (2)$$

where $\hat{y}_i$ is the estimated value of *logN* for an ith point by using the fitted line and y_i is the real value of *logN* for the ith point. $\bar{y}$ is the average value of *logN*. Index *n* denotes the last desired data to calculate the b-value.

3.3 Signal processing methods

Several features and important information are embedded in AE signals. Using signal processing methods, the inherent information can be extracted and used for the temporal assessment of features.

3.3.1 Fast Fourier transform

The Fourier transform transfers a time-series signal to a frequency domain signal by convoluting the digitized signal with sinusoidal signals ($e^{-\frac{j2\pi kn}{N}}$) with different frequencies. The following equation represents the formulation for a Fourier transform:

$$X_k = \sum_{n=0}^{N-1} x_n e^{-\frac{j2\pi kn}{N}} \quad (3)$$

where N is the number of samples, "x_n" is a signal in a time domain, and X_k is the Fourier transform coefficients for the k^{th} frequency.

3.3.2 Continuous wavelet analysis

The wavelet transform (WT) is utilized to present the energy distributions of signals in a time-frequency domain. Contrary to the windowed Fourier transform (WFT), the wavelet transform (WT) presents data in a high time resolution for the high-frequency components and a high-frequency resolution for the low-frequency components. The continuous wavelet transform (CWT) is defined according to the following equation:

$$CWT(a,b) = \int S(t) * |a|^{-0.5} \Psi\left(\frac{t-b}{a}\right) dt \quad (4)$$

where "a" and "b" are scale and shift parameters, respectively. The scale parameter controls the compactness or extension of a signal (frequency), and the shift parameter defines the position of the mobile window in the time domain. "$S(t)$" is a signal time history. Eq. (5) is referred to as the wavelet, which is the second portion of Eq. (4). The basic window function without scale and shift parameters are referred to as the mother wavelet.

$$\Psi_{a,b}(t) = |a|^{-0.5} \Psi\left(\frac{t-b}{a}\right) \quad (5)$$

The mother wavelet used in this study is the Gabor wavelet, which is based on a Gaussian function (Suzuki, et al., 1996b). The results of wavelet analysis are the wavelet coefficients for the different combinations of time and frequency which are presented in a contour diagram or spectrogram. The 3D wavelet spectrum can also be presented as a 2D picture and used as input for an image processing algorithm.

3.3.3 Shannon's entropy

Shannon's entropy or information entropy was introduced by Shannon (Shannon, 1948). This parameter quantifies the randomness of a random variable. If the probability of an event is high, the event occurrence is expected and is not shocking; therefore, it delivers very little information. This concept can be used in signal processing and acoustic emission (Chai, et al., 2018, Kahirdeh, 2014, Kahirdeh, et al., 2017, Sauerbrunn, 2016, Soltangharaei, et al., 2021a). Different methods are recommended to calculate signal entropy in the literature (Chai, et al., 2018, Kahirdeh, 2014, Kahirdeh, et al., 2016, Sauerbrunn, 2016). The methods are: voltage amplitude entropy, feature entropy, and fast Fourier transform (FFT) entropy.

In voltage entropy, the distribution of amplitude voltages of AE signals is estimated in different bins. The bin size is recommended to be as close as possible to the resolution of AE data acquisition (Chai, et al., 2018). The distribution indicates the relative frequency of voltages within different voltage intervals, and the entropy for the voltages is calculated using the following equation (Shannon entropy equation):

$$Entropy = -\sum_{i=1}^{n} P(x_i) * \log\left(P(x_i)\right) \quad (6)$$

In the equation, *n* is the number of bins in each signal. The bins defined in each signal are represented as x_i. $P(x_i)$ is the relative frequency of each bin calculated according to the signal histogram. In this method, it is assumed that the voltage alteration is constant and independent between samples. Entropies of hits can be calculated either independently or cumulatively. The former method is referred to as discrete voltage entropy (DVE), and the later method is referred to as global voltage entropy (GVE). The two procedures are illustrated in Figure 6.

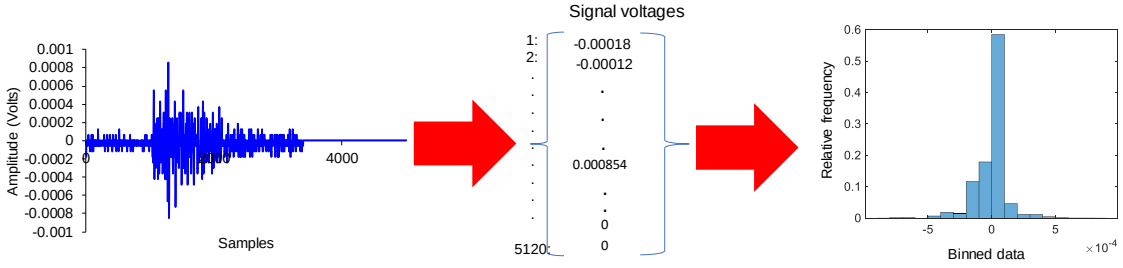

(a)

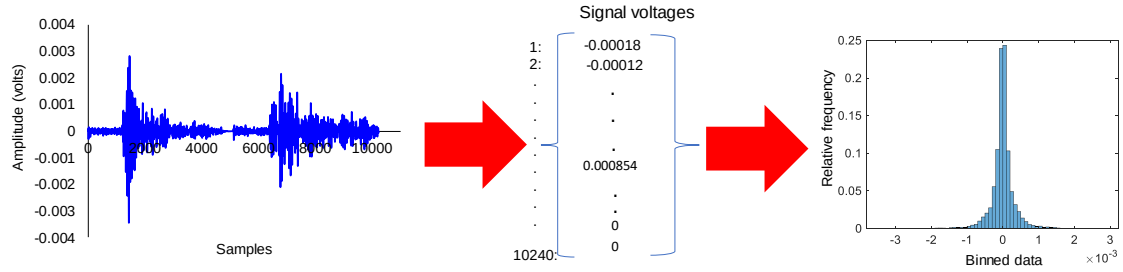

(b)

Figure 6 Voltage entropy calculated in two procedures. (a) Discrete voltage entropy; (b) Global voltage entropy (Soltangharaei, et al., 2021a).

The signals in Figure 6 have a sampling rate of 5 million samples per second. In Figure 6a, histograms are individually calculated for each hit, while in Figure 6b, histograms are calculated by considering a hit and the hits which occurred before that hit.

Counts entropy is a feature entropy, which can be calculated using two procedures. Counts in AE is defined as the number of time that signal voltage exceeds the threshold set in the system. The first method is very straightforward, and the probability is estimated by dividing the counts for each hit in a specific time by the cumulative counts of hits occurring before that time. The entropy is calculated using Eq. (6). This method is referred to as CE in this document. The second procedure is referred to as CE_CDF since the cumulative distribution function (CDF) is estimated using the empirical CDF method, and the corresponding probability distribution function (PDF) is extracted from CDF (Kahirdeh, et al., 2016). The entropy is also estimated using Eq. (6) in this method.

FFT entropy is calculated using normalized FFT spectra of signals. The normalized spectra are assumed to be probability distributions, and Shannon entropies are estimated using the FFT spectra and Eq. (6) (Kahirdeh, et al., 2016). The following figure shows how to calculate the FFT entropy.

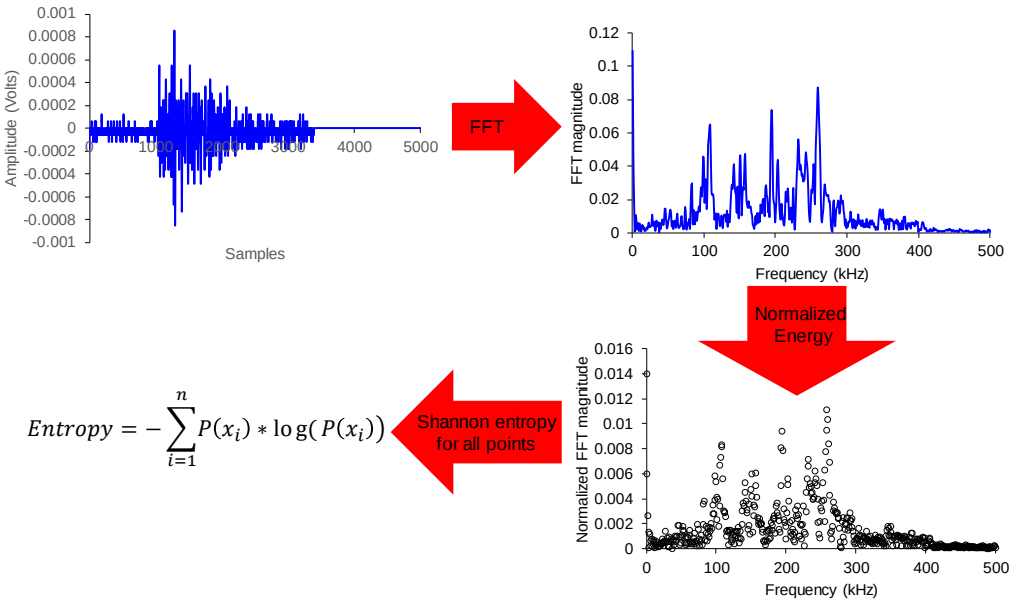

Figure 7 FFT entropy (Soltangharaei, 2020).

3.4 Machine learning and clustering methods

Machine learning and clustering methods can be categorized under data-driven methods, which are referred to as algorithms to recognize patterns and clusters in a data set as well as to predict and make decisions from new data. In the following, some common algorithms are described.

3.4.1 k-means

One of the simplest and earliest unsupervised classification methods is k-means clustering. The algorithm starts with selecting k centroids (number of clusters), which is a user-defined parameter. Then each data set is assigned to the nearest centroid, forming new clusters. The centroids are recalculated based on the new clusters. This process is repeated, and the centroid points are updated until the difference between the new centroid points and the previous points becomes negligible (Tan, et al., 2013). Figure 8 shows how the algorithm works in a 2D space.

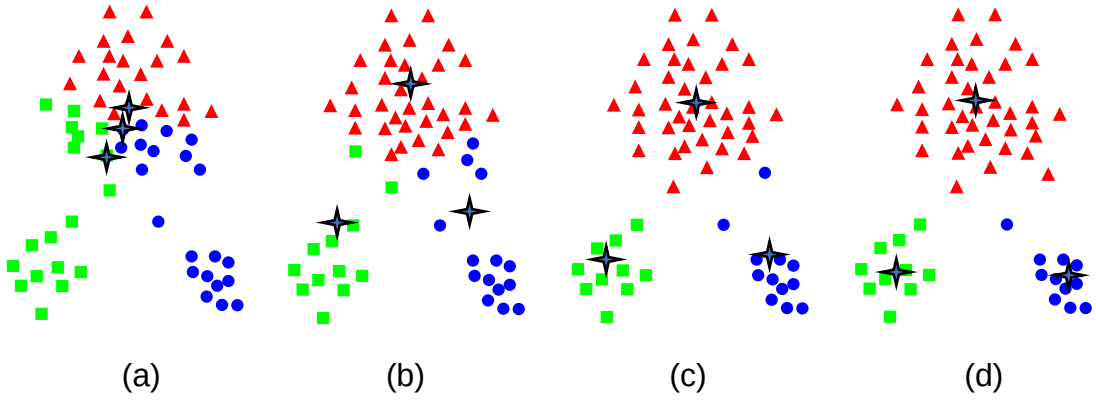

Figure 8 Schematic figure of k-means algorithm for three clusters. (a) Iteration 1; (b) Iteration 2; (c) Iteration 3; (d) Iteration 4 (Tan, et al., 2013).

The initial guess for the centroids of clusters is influential on the results of classification. The common method to start the algorithm is randomly selecting the centroid, which sometimes results in a poor classification. There are some methods recommended to improve the initial guess. One of the methods is randomly selecting the initial centroids several times and choosing the best arrangement of centroids with the lowest average cluster error. The other method is taking a sample of data and clustering them using hierarchical clustering. This method performs well if the data set is not large (a few hundreds to few thousands) and the number of desired clusters is small in comparison to the data set (Tan, et al., 2013). Another common method is selecting the farthest point from the initially selected centroids. The latter method might not be effective when the data set has outliers (Abdelrahman, et al., 2018). After selecting initial centroids, the distance between data and centroids is calculated using a proximity measure and assigning each data point to the closest centroid point. The centroids in the clusters are calculated using the following equation:

$$c_i = \frac{1}{m_i} \sum_{x \in C_i} x \tag{7}$$

Where, m_i is the number of data point in the i^{th} cluster (C_i) and x is the data point in a defined space for clustering, c_i is centroid for the i^{th} cluster (C_i). The objective function for optimization in Euclidian space might be the sum of square error (SSE) within the clusters. A lower error for each classification indicates the higher performance of clustering and less scattering in the resulted clusters (Tan, et al., 2013).

3.4.2 Agglomerative hierarchical clustering

The agglomerative hierarchical algorithm is an unsupervised pattern recognition approach, which includes three main steps: distance calculation, grouping data into clusters, and determining the number of clusters.

The result of the hierarchical clustering is usually presented in a tree-like graph called a dendrogram. The most important part of the algorithm is calculating the proximity between two clusters. Different methods are used to calculate the proximity between the clusters such as: a single link, which calculates the distance between the closest two points in two clusters; a complete link, which calculates the proximity between the farthest points in two clusters and; a group average, which calculates the average distance between the points in two clusters. In addition to the methods mentioned, Ward's method can also be utilized to calculate the proximity. In this method, clusters are presented by their centroids, and the criterion for merging two clusters is to minimize the sum of the squared distances of points in the clusters (Murtagh and Legendre, 2014). The number of clusters is determined based on the height of each link with respect to the average height of the links underneath the data dendrogram (Bouguettaya, et al., 2015). The procedure for the agglomerative hierarchical clustering is shown in a flowchart in Figure 9.

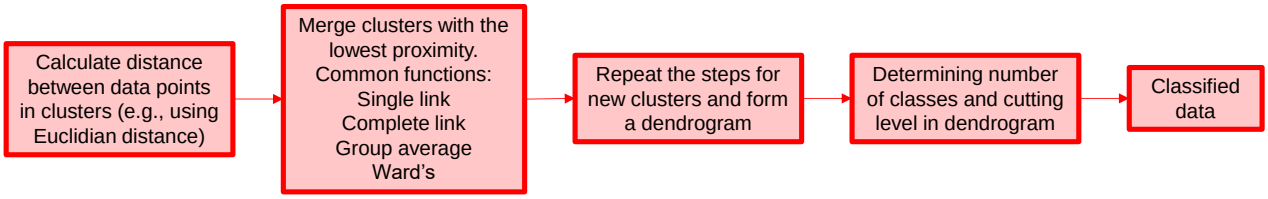

Figure 9 Agglomerative hierarchical clustering

3.4.3 Principal component analysis

Principal component analysis (PCA) is a method to reduce dimentionality of a data set. Many features can be extracted from AE signals, such as duration, counts, amplitude, peak frequency, energy, etc. However, working with all features and finding the relation between them is difficult. PCA can reduce the dimensionality of a data set by projecting the data on new coordinates. Input for a PCA is a matrix where columns are features (variables)

and rows are observations (hits). PCA initially calculates a covariance of the input matrix. Then, eigenvalue analysis is conducted on the covariance matrix, resulting in eigenvalues and eigenvectors. The number of eigenvalues and eigenvectors is the same as the number of features in the input matrix. The eigenvectors have components equal to the number of features. The eigenvalues and corresponding eigenvectors are sorted from the largest to smallest values. Then, the original input matrix is transferred to the new space by multiplying a matrix, which contains all eigenvectors. According to the eigenvalues, the least important principal components can be deleted without losing a significant amount of information.

3.4.4 Artificial neural network

Artificial neural network (ANN) can be considered as a supervised pattern recognition approach, which is trained by using labeled data to classify new unlabeled data or to estimate values according to new input data.

Multilayer ANNs have three main layers: input, hidden, and output layers. The intermediary layers between input and output layers is referred to as hidden layers, where ANN learns the relationship between input and target data (Solomatine, et al., 2009). The algorithm aims to solve an optimization problem to make an output of ANN as close as possible to the target values. In this procedure, weight factors for each neuron are frequently updated to reach the target values. A schematic architecture of a multilayer ANN is shown in Figure 10.

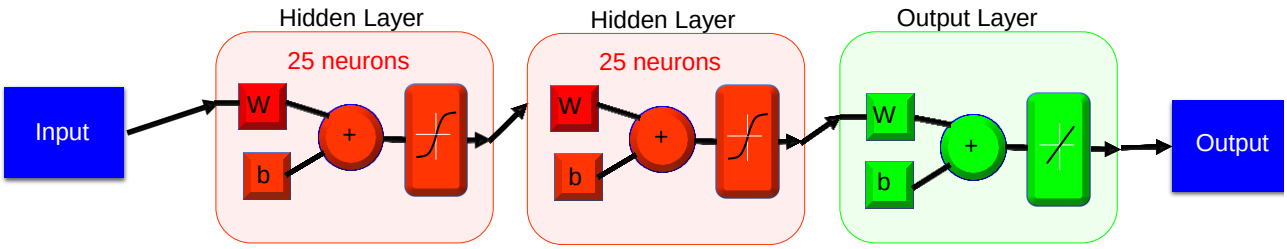

Figure 10 Schematic artificial neural network with two hidden layers (Soltangharaei, et al., 2020b).

The input and target data are given to an ANN model. The ANN algorithm starts iteration by initial weight values (randomly selected) and computes output values, and compares it with target values given to the model. Errors are calculated, and weight vectors are updated accordingly. This procedure continues until the output values approach the target values as closely as possible. Nonlinear activation functions such as sigmoid or hyperbolic tangent functions can be employed to produce a nonlinear relationship between target and input values (Tan, et al., 2018).

The input data is usually separated into three data sets: training, validation, and test data. The training data set is utilized for training the network. The validation data is selected from the input data to evaluate the network during the training process. This data is utilized to help a network to be generalized for a new dataset. The testing data is an independent dataset to test the performance of the trained network (Gavin, 2011).

3.4.5 Stacked autoencoder neural network

This algorithm is a deep learning method. Deep learning networks have the ability to extract features from raw data rather than using prepared features. Deep learning methods can be used in computer vision, audio processing, signal processing, and language processing.

Each autoencoder has three layers similar to ANN: input, hidden, and output layers. Autoencoders are an unsupervised learning network, which discovers the embedded pattern in a data set by condensing the original input data and reconstructing the data set from the condensed data (Shin, et al., 2012). A schematic structure of an autoencoder layer is shown in Figure 11. The structure of the autoencoder is a bottleneck-shape in the hidden layer, as seen in the figure.

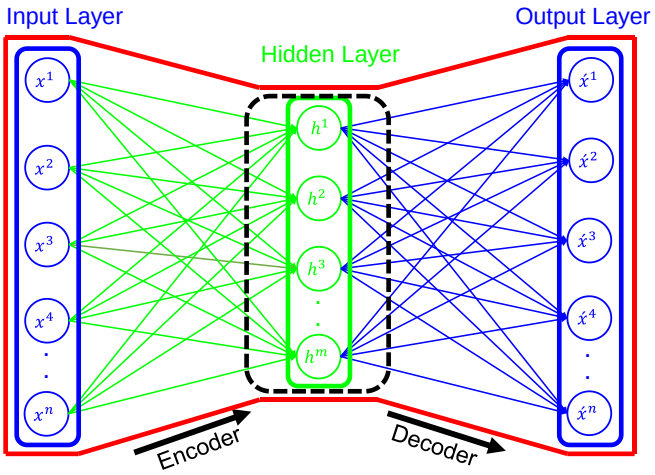

Figure 11 Autoencoder structure.

If the input data has *n* dimensions $\{x^1, x^2, x^3 \dots x^n\}$ and the hidden layer has *m* dimensions, where *m*<*n*, the input data will be condensed using a nonlinear encoding function. The result of encoding is going through a decoding function and reconstructed in the output layer ($\{x'^1, x'^2, x'^3 \dots x'^n\}$). The encoding (*E*) and decoding (*D*) functions can be presented in the following equations:

$$E(x) = S_\theta(wx + b) \tag{8}$$

$$D(h) = S_{\theta'}(\mathrm{w}'h + b') \quad (9)$$

In the above equations, w and w' are weights of encoder and decoder functions, and each is a $m \times n$ matrix. b and b' are bias vectors for encoder and decoder functions. The activation functions can be sigmoid, hyperbolic tangent functions, or a customized function. An autoencoder's objective is to minimize the error between the original data and the reconstructed version of the data.

A stacked autoencoder network can be built by stacking two or several autoencoders (Wang, et al., 2019). The first autoencoder derives the features from the input data. The features from the first autoencoder are the input for the next autoencoder. New features are then extracted from the second autoencoder. This procedure will be continued up to the last autoencoder. The resulted features from the last autoencoder layer are used as an input for either the classification, using a softmax layer or prediction using a regression layer. This part of the stacked autoencoder is supervised, and the network is trained for the assigned labels or values. The network can be fine-tuned by backpropagation to improve the performance of the network (Wang, et al., 2019). A schematic structure of a stacked autoencoder with two autoencoders is shown in Figure 12. As seen in the figure, AE waveforms or FFT spectra of AE can be used as an input data set for a stacked autoencoder.

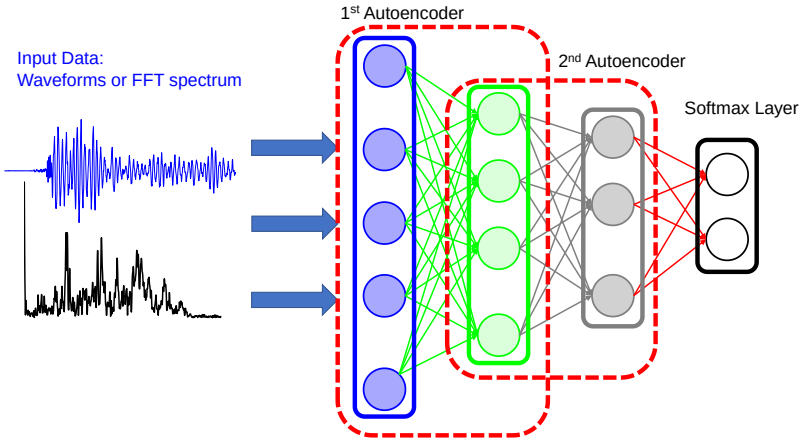

Figure 12 Stacked autoencoder network with two autoencoders and classification layer.

3.4.6 Convolutional neural network

A convolutional neural network (CNN) is a deep learning method mostly used for image and signal recognition (Krizhevsky, et al., 2012a). The main components of a convolutional neural network are an input layer, feature extraction layers, and a fully connected layer. A schematic CNN structure is illustrated in Figure 13.

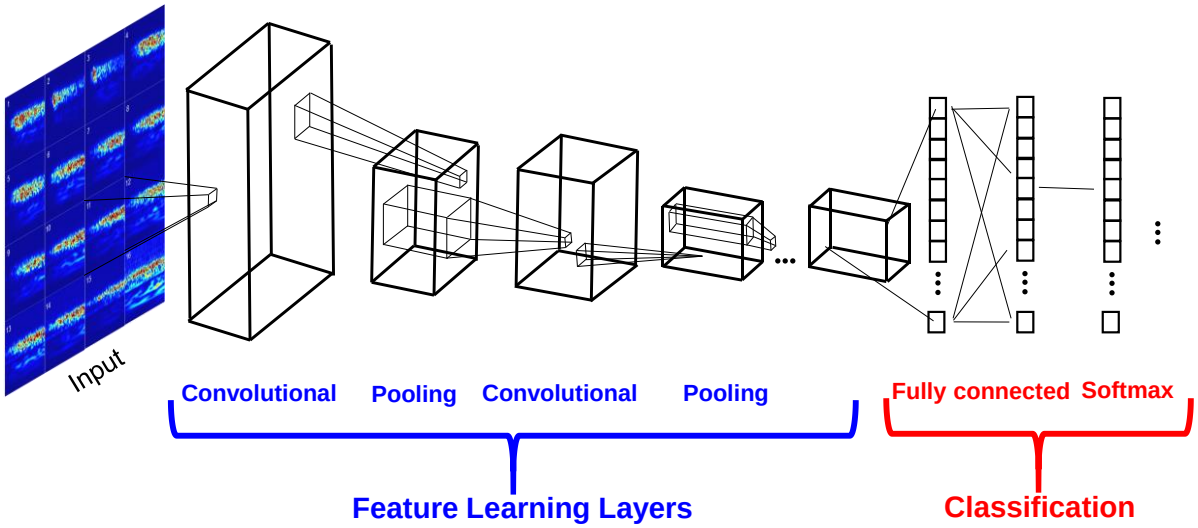

Figure 13 A simplified CNN structure for wavelet contour classification.

The input data for picture classification is a tensor with (number of images) × (image height) × (image width) × (input channels) and is usually divided into training and testing data sets. Feature extraction layers include convolutional and pooling layers. In the feature extraction layers, the algorithm extracts features and learns to differentiate them. AE data can be presented as images using a wavelet transform. The resulting images are inserted as an input set in a CNN. Each picture goes through several convolutional filters, which highlight specific features of the picture.

In a convolutional layer, several kernels (filters) are utilized to filter the input data and extract features. For instance, the output of the j^{th} feature map in the n^{th} convolutional layer is calculated by the following equation:

$$x_j^n = f\left(\sum_{i=1}^{M} x_i^{n-1} * k_{ij}^n + b_j^n\right) \tag{10}$$

Where, *f( )* is an activation function, "*" indicates convolution between the data and kernels, k_{ij}^n is the kernel of the n^{th} filter, b_j^n is the bias parameter for the n^{th} filter, x_i^{n-1} is the input feature map from the previous convolutional layer $(n\text{-}1)^{th}$.

The pooling layer takes samples of feature maps from the previous convolutional layer and reduces the size of features (Sun, et al., 2020). If the down-sampling is not conducted from layer to layer, the computation process becomes expensive, and the model is prone to overfitting. Therefore, a pooling layer is required after

each convolutional layer. The down-sampling can be conducted either using maximum pooling or average pooling. The general function for the pooling layer is as follows:

$$x_j^n = f\left(\beta_j^n s_{down}(x_j^{n-1}) + b_j^n\right) \quad (11)$$

In the equation, *f( )* is the activation function, β_j^n and b_j^n refers to the multiplicative and additive bias, S_{down} is the down-sampling function, x_j^{n-1} is the input feature map, x_j^n is the output after down-sampling.

The fully connected layer is usually placed at the end of the network and transfers all features from the last pooling layer to a feature vector. The function for the fully connected layer has w^j weight and b^j bias as indicated below:

$$x^j = f\left(x^{j-1}w^j + b^j\right) \quad (12)$$

f is the activation function for the fully connected layer, x^{j-1} and x^j are input and output of the layer.

Convolutional neural networks have several parameters and complex structures. Designing and training a CNN from the beginning is very challenging and time-consuming and requires a large amount of data. Therefore, a concept of transfer learning was introduced to overcome the challenges with a new CNN (Pan and Yang, 2009). The transfer learning is based on a CNN that was already been trained by a large amount of data. The pre-trained network is fed by the new data (pictures) through the deeper layer of CNN. Learning rates for the initial layers (transferred layers) should be extremely decreased, and the learning rate factors for the fully connected layer should be increased. Some famous pre-trained CNNs for transfer learning are GoogLeNet (Szegedy, et al., 2015), AlexNet (Krizhevsky, et al., 2012b), ResNet (He, et al., 2016), and Inception-v3 (Szegedy, et al., 2016).

4 Case studies

In this section, some examples using data-driven methods in AE data are discussed.

4.1 Stress corrosion cracking

The application of AE in monitoring the damage caused by SCC in stainless steel has been presented by several researchers (Shaikh, et al. 2007; Alvarez, et al. 2008; Du, et al. 2011; Xu, et al. 2012; Kovač, et al. 2015). Some researchers focused on the fracture modes and signal differences between intergranular and transgranular cracking mechanisms (Alvarez, et al., 2008). Recently, a research study was conducted regarding the capability of AE to recognize and localize SCC on stainless steel plates, which resembled a DCSS structure material at the

University of South Carolina. Figure 14 shows large-scale and small-scale specimens, used for SCC tests. The large specimen is 5029 mm × 1524 mm × 16 mm and has four notches. The small-scale specimen is 305 mm × 311 mm × 16 mm with a single notch.

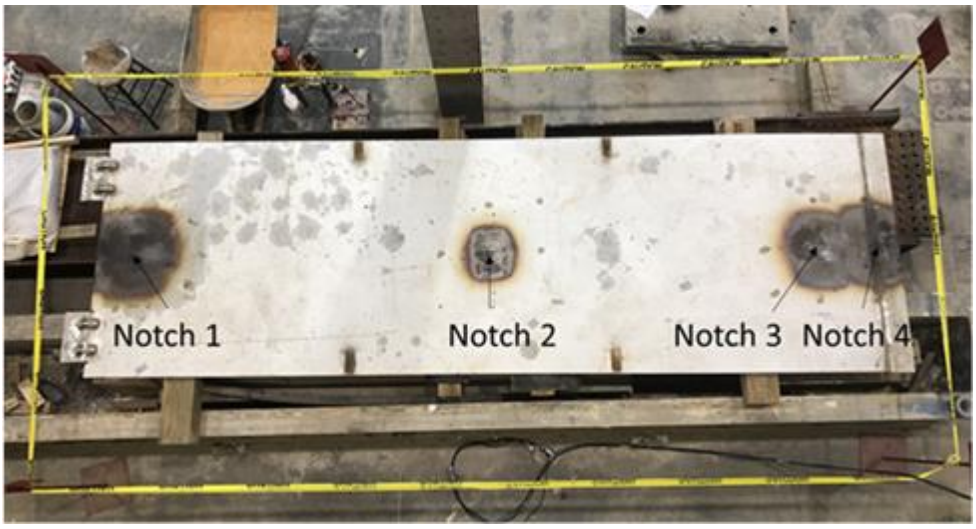

(a)

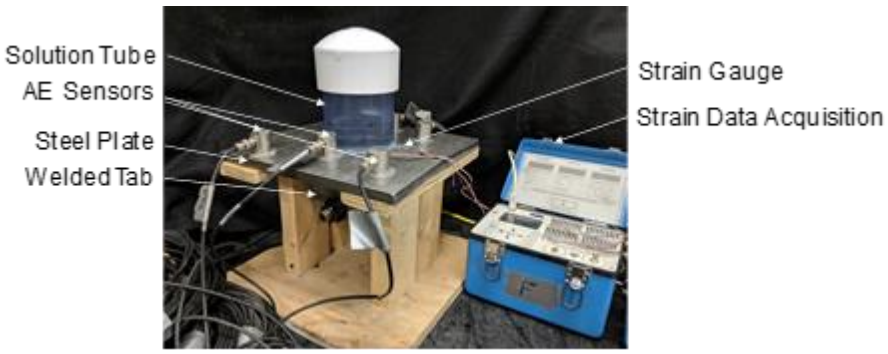

(b)

Figure 14 (a) Large-scale stainless-steel plate; (b) Small-scale stainless-steel plate (Ai, et al., 2021a, Soltangharaei, et al., 2020c).

A potassium tetrathionate (K2S4O6) solution was used as an electrolyte to provide a corrosive environment at the notch locations. A plastic tube was placed on the notches and the solution was poured inside. The pH of the solution was decreased by adding sulfuric acid, which expedited the corrosion reaction. The top surface of the steel plates at the location of each notch was exposed to tensile stress by applying out-of-plane bending. The steel plates were heat-treated before the test for sensitization purposes, as shown in Figure 1. The first visible crack was observed on the 9th day of the experiment, as shown in Figure 15.

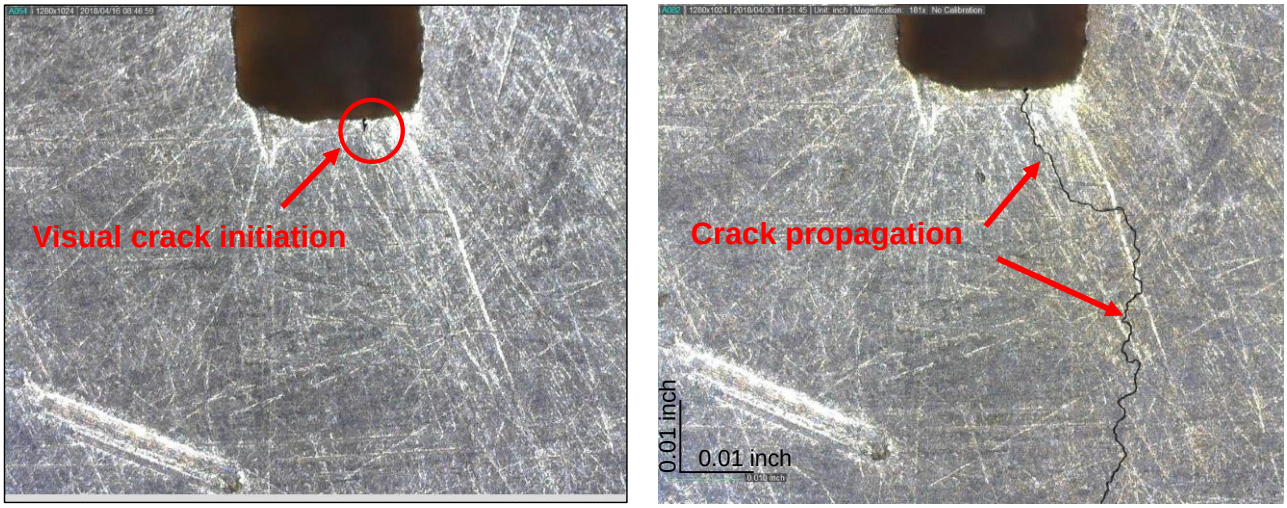

(a) (b)

Figure 15 Visual cracking: (a) Initiation at 9th day; (b) Crack propagation at 19th day (Soltangharaei, et al., 2020c).

The signals were transferred to the frequency domain using FFT. The areas under FFT spectra were divided in terms of frequency intervals. Energies enclosed in the frequency intervals were estimated. For example, the Nyquist frequency, which was 500 kHz, was divided into ten equal intervals. Therefore, ten energy values were calculated and used as the signal features. PCA was conducted on the data to reduce the dimension of the data set. The first four principal components, which accounted for 93% of the cumulative variance, were selected for pattern recognition. An agglomerative hierarchical clustering method was used to classify the data based on the new features derived from PCA, and Ward's was used to estimate the similarity and link the objects (Murtagh and Legendre, 2014). The classified data was illustrated in terms of the first three principal components in 3D space in Figure 16.

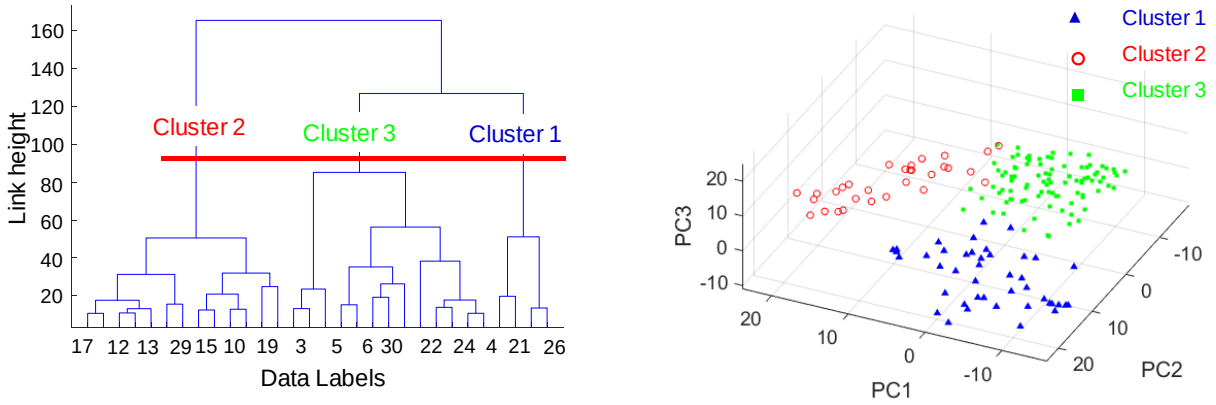

(a) (b)

Figure 16 (a) Clustering dendrogram; (b) Data in principal component space (Soltangharaei, et al., 2020c).

Average energy distributions in terms of frequency and cumulative signal strength in terms of experimental time for the three clusters are shown in Figure 17.

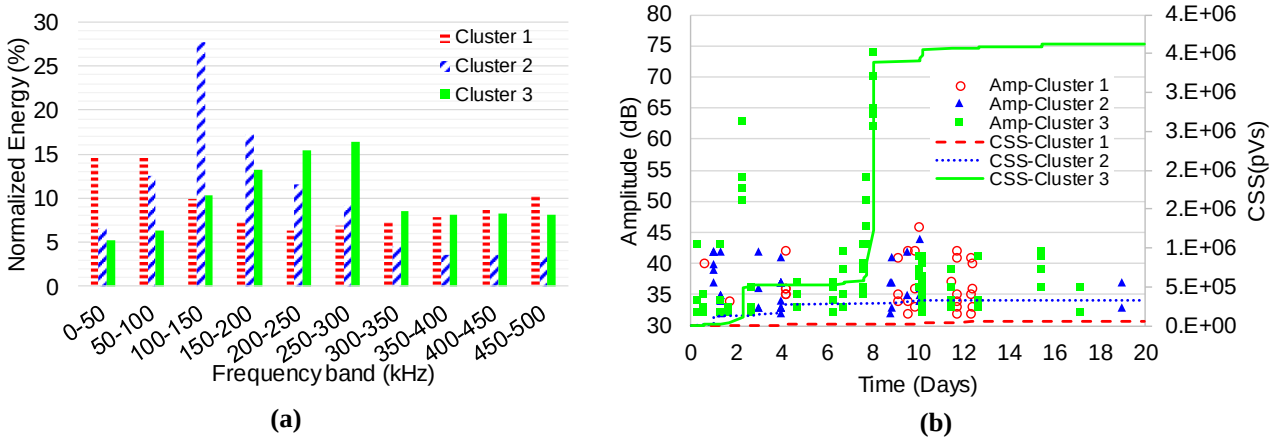

Figure 17 (a) Average energy distribution; (b) Amplitude and CSS versus time for classified data (Soltangharaei, et al., 2020c).

The major jump in CSS occurred on the 8th day, which was close to the day (9th day) that the crack initiation was visually observed (Figure 17b). Furthermore, Cluster 3 has the largest energy accumulation in frequencies higher than 200 kHz (Figure 17a), and is the largest contributor in the major CSS jump (Figure 17b).

Coefficients of determination calculated from the global b-values in some instances during the test are presented in Figure 18. A temporal trend is observed in the figure, where the increase in the coefficients of determination was followed by a sharp decrease after the first visible crack.

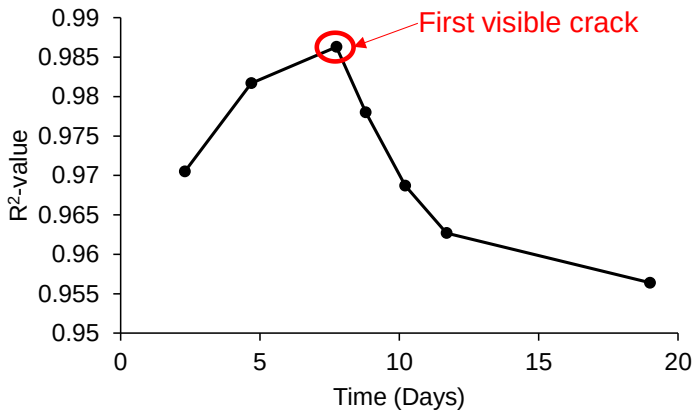

Figure 18 Coefficient of determination evolution during the SCC test for global b-value (Soltangharaei, et al., 2020c).

ANN and stacked autoencoder can be utilized for zonal localization in large-scale structures using minimal sensor numbers (Ai, et al., 2021a). The inputs for the ANN model were parametric features such as

duration, amplitude, rise time, average frequency, root mean square, energy, and peak frequency. However, the input dataset for the stacked autoencoder model was AE waveforms (time series). The large-scale plate was divided into five zones, as shown in Figure 19a. The source location results indicated a significant improvement using the stacked autoencoder in Figure 19b.

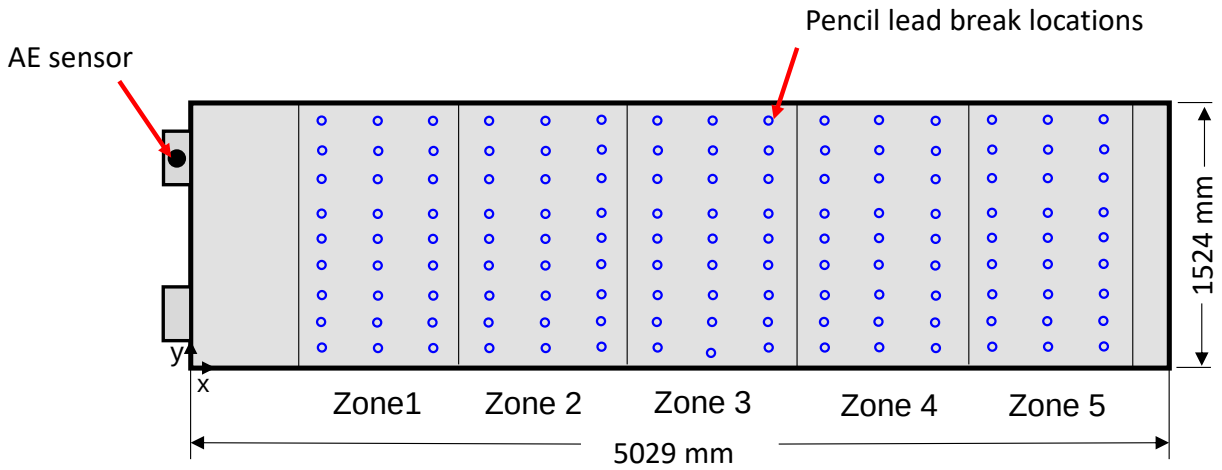

(a)

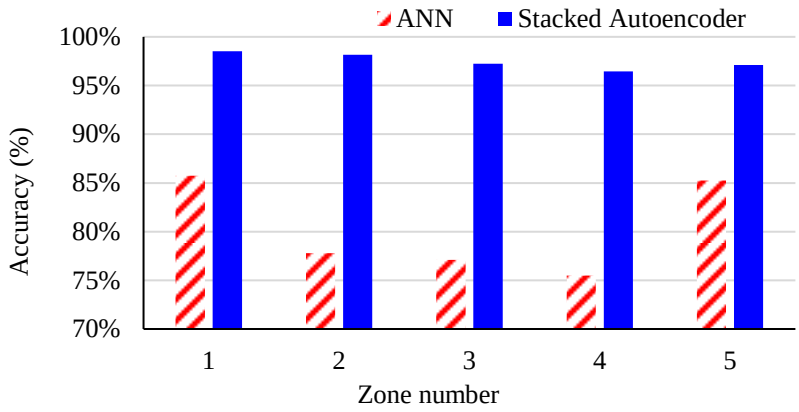

(b)

Figure 19 (a) Zones on large-scale plate; (b) Zonal localization accuracy for ANN and stacked autoencoder (Ai, et al., 2021a).

4.2 Alkali-silica reaction

Several recent bodies of research have focused on using acoustic emission to monitor the ASR degradation of concrete structures (Abdelrahman, et al., 2015, Farnam, et al., 2015, Lokajíček, et al., 2017, Pour-Ghaz, et al., 2012, Soltangharaei, et al., 2021a, Soltangharaei, et al., 2020a, Soltangharaei, et al., 2018). The ability of AE to record stress waves emitted during ASR was initially discussed by Pour-Ghaz, et al. (2012), and a correlation between cumulative signal strength and ASR expansion was later discussed by Abdelrahman, et al. (2015).

Farnam, et al. (2015) discussed the frequency content of AE signals emitted during ASR using feature analysis. They compared the frequency content of AE during ASR with the AE data acquired from fracture tests. Lokajíček, et al. (2017) discussed the relationship between the reactivity of aggregates and AE energy.

Several investigations were conducted by the University of South Carolina regarding ASR in reinforced and unreinforced concrete and large-scale specimens (Soltangharaei, et al., 2021a, Soltangharaei, et al., 2020a, Soltangharaei, et al., 2018). Agglomerative hierarchical pattern recognition in combination with PCA were utilized to classify the AE data in terms of frequency-energy features extracted from FFT spectra. Furthermore the temporal evolution of data for different clusters was evaluated in both large-scale and medium-scale specimens.

Spacial statistical distributions of AE events are used to identify the difference between damage mechanisms of structures with and without confinements (Soltangharaei, et al., 2020a). The following figure presents the contour tomographies of AE events for the confined and unconfined specimens. According to Figure 20 and Figure 5, the pattern of event distribution for the confined specimen is different from the unconfined specimen. The events for the confined specimen mostly occurred in the mid-third portion of the specimen width (Y direction) compared to the unconfined specimen.

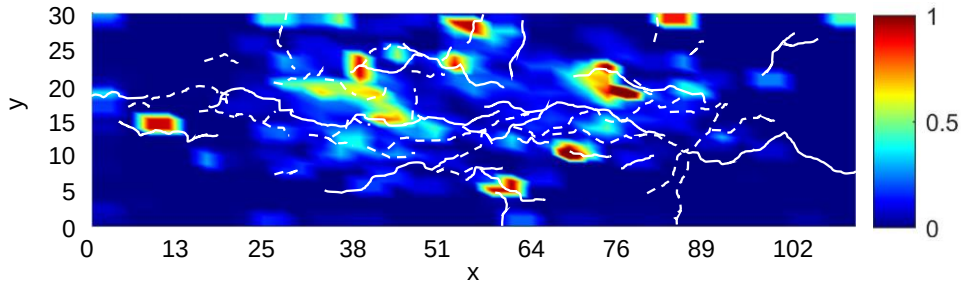

(a)

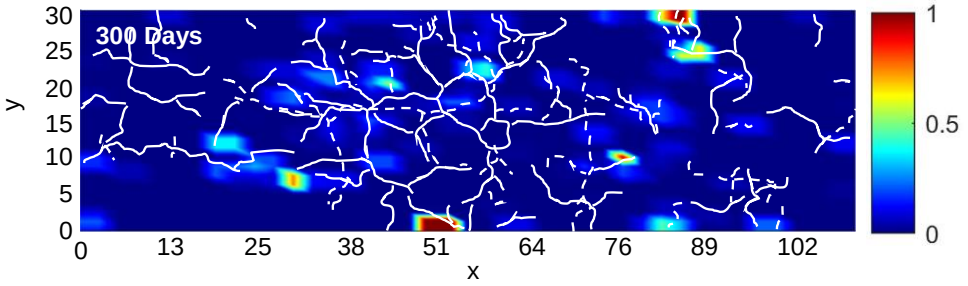

(b)

Figure 20 AE event tomography: (a) confined specimen; (b) unconfined specimen (Soltangharaei, et al., 2020a).

The probabilities of event occurrence in the mid-third region of the specimen width were calculated at different instances during ASR for both specimens and shown in Figure 21.

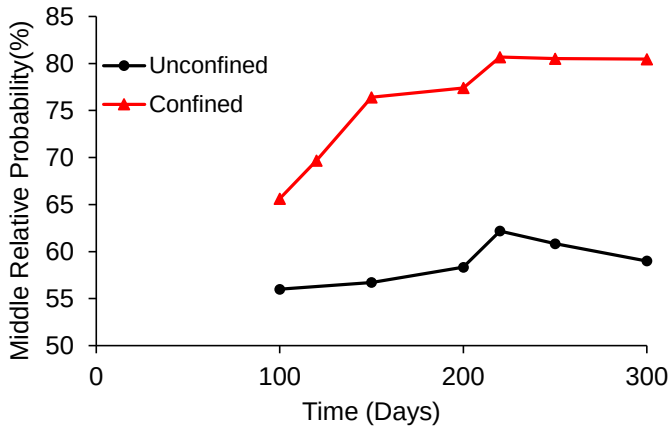

Figure 21 Temporal evolution of middle relative probability of events for confined and unconfined specimens.

Shannon entropy can be employed to discriminate different phases during ASR, as mentioned in section 3.3.3. The results of counts entropy using CDF (CE_CDF) for the confined and unconfined specimens are shown

in Figure 22. The entropy is initially increased and followed by a gradual decrease. In other words, the randomness of the data is rising during the first stage, which can be attributed to the microcrack formation in the concrete specimen. As ASR proceeds, the microcracks coalesce and form macrocracks in specific locations, decreasing the randomness of the data.

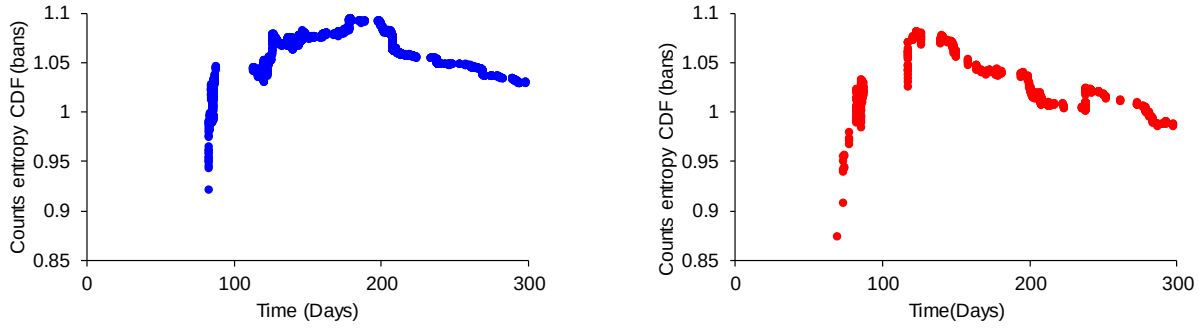

(a) (b)

Figure 22 Counts entropy for: (a) confined; (b) unconfined specimens (Soltangharaei, et al., 2021a).

4.3 Impact on an airplane elevator

Fiber carbon composite materials are used in aerospace structures such as airplanes due to their high strength and low density. However, this material may be susceptible to the impacts of debris and hail. Therefore, a structural health monitoring system, which can localize and determine impact levels, is essential for safe operation.

A zonal localization model based on data-driven methods was developed using a pattern recognition method and ANN (Soltangharaei, et al., 2019b). The data was collected through a single broadband AE sensor (attached to the elevator spar) by impacting the surface of the structure using the steel impactors shown in Figure 3. The impact locations are shown in Figure 23c. K-means and PCA were used to classify the data along the elevator. Parametric features such as duration, rise time, signal strength, average frequency, amplitude, counts, and counts to peak were utilized for classification. The features evolved as the impact source moved farther from the sensor. PCA was conducted on the parametric features to reduce the data dimensions (Figure 23b). The data is shown in Figure 23b in a 2D principal component space. The resulting principal components were utilized as data features in the k-means method. The algorithm classified the data into three clusters, indicating the boundary of zones for the zonal source location model (Figure 23a).

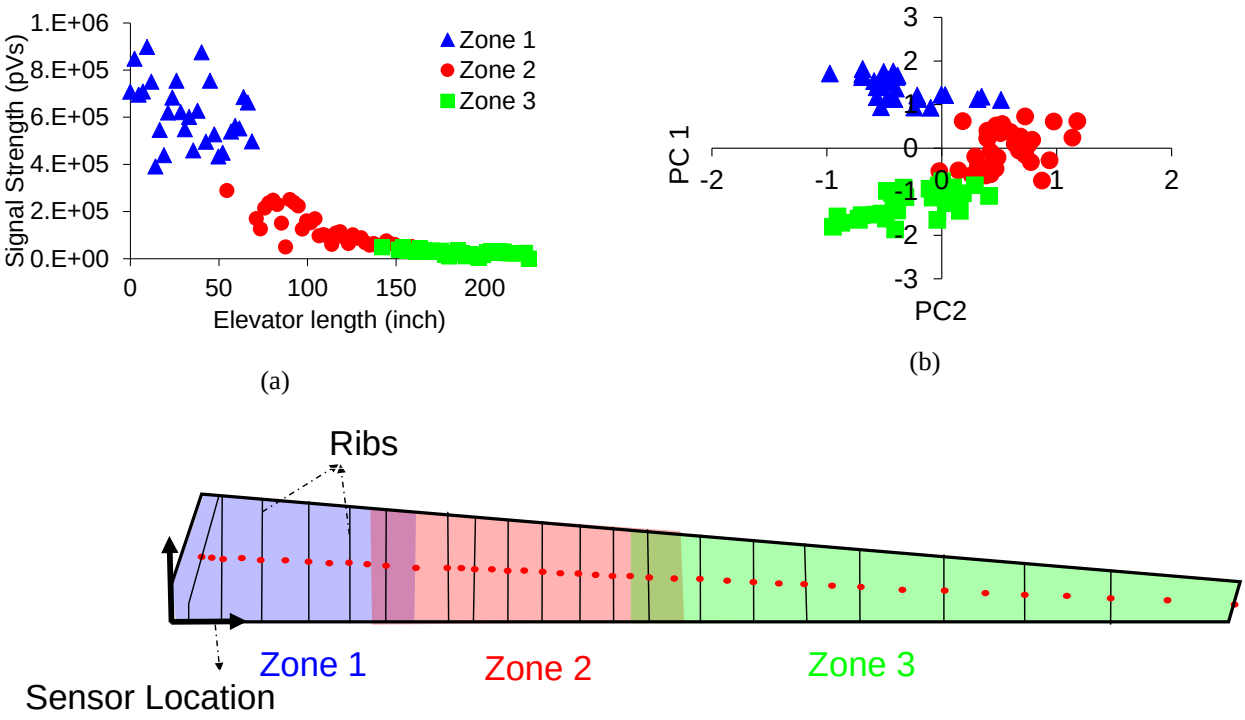

Figure 23 K-means result: (a) signal strength variation of AE data along elevator; (b) PCA; (c) zone boundaries (Soltangharaei, et al., 2019b).

The data was labeled based on the k-means results (zone 1, zone 2, zone 3). The labeled data was then fed into an ANN model that was developed with two hidden layers (25 neurons in each layer) and a regression output layer. The data set was divided into three subsets of training, validation, and testing. The ANN was trained several times to get an optimum result with the lowest testing errors. The trained ANN can be used to estimate the zonal location of impacts on the elevator. The features from any of the impacts can be used as input for the model. The model result will be a zone number. The mislocalization error is reduced by considering overlaps in the zone boundaries (Figure 23c) as shown in Figure 24.

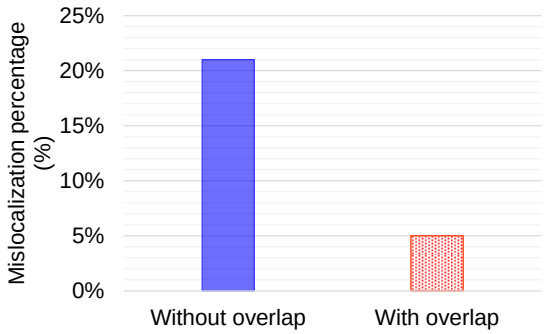

Figure 24 ANN error for zonal source localization of elevator.

Deep learning methods such as autoencoder networks can be used to develop a zonal source location model for the elevator using raw data (signals in time or frequency domains) and are expected to have more precise results for a model with a larger zone number, as discussed in (Ai, et al., 2021a), for a large-scale steel plate and elevator (Ai, et al., 2021b). However, computation and training time for deep learning is much larger than ANN models. In addition, larger data storage is required for the input data of deep learning methods. These two drawbacks bring limitations for on-flight data acquisition and decision making systems, making ANN models more suitable for this specific application at this point in time.

5 Conclusions and recommendations

AE is a nondestructive method to detect damage in different structures due to different mechanisms. One of the advantages of this method compared to other methods is the high sensitivity of AE sensors, which result in obtaining more data from micro-scale to macro-scale damages. This advantage brings challenges in terms of data analysis and management. The challenges can be attributed to the collection of extraneous data during acquisition or may be related to data analysis and interpretation. The former is resolved by providing different filtering approaches and protecting electrical connections, while the latter can be handled by different data-driven methods, some of which are presented in this chapter. The case studies illustrate the applications of some analysis methods for the AE data acquired from different loading or stress conditions applied to steel, concrete, and fiber reinforced composite structures.

Implementing more complex algorithms and data-driven models to analyze AE data becomes more feasible as computational hardware and systems advance. In addition, these methods can be a step forward in the development of an integrated autonomous system for data acquisition, data analysis, data interpretation,

structural condition estimation, and decision making. Deep learning algorithms such as CNN, autoencoder, and recurrent neural networks such as long short-term memory (LSTM) networks are recommended to be employed for analyzing complex AE data as well as estimating dependencies of data in a time domain.

References

Abdelrahman, M., ElBatanouny, M., Dixon, K., Serrato, M., and Ziehl, P. (2018). "Remote Monitoring and Evaluation of Damage at a Decommissioned Nuclear Facility Using Acoustic Emission." *Applied Sciences*, 8(9), 1663.

Abdelrahman, M., ElBatanouny, M. K., Ziehl, P., Fasl, J., Larosche, C. J., and Fraczek, J. (2015). "Classification of alkali–silica reaction damage using acoustic emission: A proof-of-concept study." *Construction Building Materials*, 95, 406-413.

Abdelrahman, M., ElBatanouny, M. K., and Ziehl, P. H. (2014). "Acoustic emission based damage assessment method for prestressed concrete structures: Modified index of damage." *Engineering Structures*, 60, 258-264.

Abdelrahman, M. A., ElBatanouny, M. K., Rose, J. R., and Ziehl, P. H. (2019). "Signal processing techniques for filtering acoustic emission data in prestressed concrete." *Research in Nondestructive Evaluation*, 30(3), 127-148.

Ai, L., Soltangharaei, V., Bayat, M., Greer, B., and ziehl, P. (2021a). "Source localization on large-scale canisters for used nuclear fuel storage using optimal number of acoustic emission sensors " *Nuclear Engineering and Design*, 375, 111097.

Ai, L., Soltangharaei, V., Bayat, M., van Tooren, M., and Ziehl, P. (2021b). "Detection of impact on aircraft composite structure using machine learning techniques." *Measurement Science Technology*.

Allard, A., Bilodeau, S., Pissot, F., Fournier, B., Bastien, J., and Bissonnette, B. (2018). "Expansive behavior of thick concrete slabs affected by alkali-silica reaction (ASR)." *Construction Building Materials*, 171, 421-436.

Alvarez, M., Lapitz, P., and Ruzzante, J. (2008). "AE response of type 304 stainless steel during stress corrosion crack propagation." *Corrosion Science*, 50(12), 3382-3388.

An, D., Kim, N. H., and Choi, J.-H. (2015). "Practical options for selecting data-driven or physics-based prognostics algorithms with reviews." *Reliability Engineering & System Safety*, 133, 223-236.

Anay, R., Lane, A., Jáuregui, D. V., Weldon, B. D., Soltangharaei, V., and Ziehl, P. (2020). "On-Site Acoustic-Emission Monitoring for a Prestressed Concrete BT-54 AASHTO Girder Bridge." *Journal of Performance of Constructed Facilities*, 34(3), 04020034.

Anay, R., Soltangharaei, V., Assi, L., DeVol, T., and Ziehl, P. (2018). "Identification of damage mechanisms in cement paste based on acoustic emission." *Construction Building Materials*, 164, 286-296.

ASTM, E. (2006). "Standard terminology for nondestructive examinations."

Barbosa, R. A., Hansen, S. G., Hansen, K. K., Hoang, L. C., and Grelk, B. (2018). "Influence of alkali-silica reaction and crack orientation on the uniaxial compressive strength of concrete cores from slab bridges." *Construction Building Materials*, 176, 440-451.

Bažant, Z. P., and Steffens, A. (2000). "Mathematical model for kinetics of alkali–silica reaction in concrete." *Cement Concrete Research*, 30(3), 419-428.

Bishop, C. M. (2006). *Pattern recognition and machine learning*, springer.

Bouguettaya, A., Yu, Q., Liu, X., Zhou, X., and Song, A. (2015). "Efficient agglomerative hierarchical clustering." *Expert Systems with Applications*, 42(5), 2785-2797.

Chai, M., Zhang, Z., and Duan, Q. (2018). "A new qualitative acoustic emission parameter based on Shannon's entropy for damage monitoring." *Mechanical Systems Signal Processing*, 100, 617-629.

Colombo, I. S., Main, I., and Forde, M. (2003). "Assessing damage of reinforced concrete beam using "b-value" analysis of acoustic emission signals." *Journal of Materials in Civil Engineering*, 15(3), 280-286.

Dron, R., and Brivot, F. (1992). "Thermodynamic and kinetic approach to the alkali-silica reaction. Part 1: Concepts." *Cement Concrete Research*, 22(5), 941-948.

ElBatanouny, M. K., Ziehl, P. H., Larosche, A., Mangual, J., Matta, F., and Nanni, A. (2014). "Acoustic emission monitoring for assessment of prestressed concrete beams." *Construction Building Materials*, 58, 46-53.

Farnam, Y., Geiker, M. R., Bentz, D., and Weiss, J. (2015). "Acoustic emission waveform characterization of crack origin and mode in fractured and ASR damaged concrete." *Cement and Concrete Composites*, 60, 135-145.

Fowler, T. J., Blessing, J. A., Conlisk, P. J., and Swanson, T. L. (1989). "The MONPAC system." *Journal of acoustic emission*, 8(3), 1-8.

Gavin, H. (2011). "The Levenberg-Marquardt method for nonlinear least squares curve-fitting problems."

Hanson, W. "Studies Relating To the Mechanism by Which the Alkali-Aggregate Reaction Produces EXPANSION IN CONCRETE." *Proc., Journal Proceedings*, 213-228.

Hawkins, D. M. (1980). *Identification of outliers*, Springer.

Hayashi, C. (1998). "What is data science? Fundamental concepts and a heuristic example." *Data Science, Classification, and Related Methods*, Springer, 40-51.

He, K., Zhang, X., Ren, S., and Sun, J. "Deep residual learning for image recognition." *Proc., Proceedings of the IEEE conference on computer vision and pattern recognition*, 770-778.

Jun, S. S., and Jin, C. S. J. K. J. o. C. E. (2010). "ASR products on the content of reactive aggregate." 14(4), 539-545.

Jung, D. Y., Mizutani, Y., Todoroki, A., and Suzuki, Y. (2017). "Frequency Dependence of the b-Value Used for Acoustic Emission Analysis of Glass Fiber Reinforced Plastics." *Open Journal of Composite Materials*, 7(03), 117.

Kahirdeh, A. (2014). "Energy Dissipation and Entropy Generation During the Fatigue Degradation: Application to Health Monitoring of Composites." Doctor of Philosophy, Louisiana State University.

Kahirdeh, A., Sauerbrunn, C., and Modarres, M. "Acoustic emission entropy as a measure of damage in materials." *Proc., AIP Conference Proceedings*, AIP Publishing, 060007.

Kahirdeh, A., Sauerbrunn, C., Yun, H., and Modarres, M. (2017). "A parametric approach to acoustic entropy estimation for assessment of fatigue damage." *International Journal of Fatigue*, 100, 229-237.

Karthik, M. M., Mander, J. B., and Hurlebaus, S. (2016). "Deterioration data of a large-scale reinforced concrete specimen with severe ASR/DEF deterioration." *Construction Building Materials*, 124, 20-30.

Krizhevsky, A., Sutskever, I., and Hinton, G. E. "Imagenet classification with deep convolutional neural networks." *Proc., Advances in neural information processing systems*, 1097-1105.

Krizhevsky, A., Sutskever, I., and Hinton, G. E. (2012b). "Imagenet classification with deep convolutional neural networks." *Advances in neural information processing systems*, 25, 1097-1105.

Lokajíček, T., Přikryl, R., Šachlová, Š., and Kuchařová, A. (2017). "Acoustic emission monitoring of crack formation during alkali silica reactivity accelerated mortar bar test." *Engineering geology*, 220, 175-182.

MISTRASGroup (2011). "PKWDI Sensor Wideband Low Power Integral Preamplifier Resonant Sensor." P. A. Corporation, ed., Copyright © 2011 MISTRAS Group, Inc. All Rights Reserved.

Murtagh, F., and Legendre, P. (2014). "Ward's hierarchical agglomerative clustering method: which algorithms implement Ward's criterion?" *Journal of classification*, 31(3), 274-295.

Ohtsu, M. (1995). "Acoustic emission theory for moment tensor analysis." *Research in Nondestructive Evaluation*, 6(3), 169-184.

Ott, R. L., and Longnecker, M. T. (2015). *An introduction to statistical methods and data analysis*, Nelson Education.

Pan, S. J., and Yang, Q. (2009). "A survey on transfer learning." *IEEE Transactions on knowledge data engineering*, 22(10), 1345-1359.

Ponce, J., and Batic, O. R. (2006). "Different manifestations of the alkali-silica reaction in concrete according to the reaction kinetics of the reactive aggregate." *Cement Concrete Research*, 36(6), 1148-1156.

Pour-Ghaz, M., Spragg, R., Castro, J., and Weiss, J. "Can acoustic emission be used to detect alkali silica reaction earlier than length change tests." *Proc., Proceeding of the 14th International Conference on Alkali-Aggregate Reaction in Concrete*.

Rajabipour, F., Giannini, E., Dunant, C., Ideker, J. H., and Thomas, M. D. (2015). "Alkali–silica reaction: current understanding of the reaction mechanisms and the knowledge gaps." *Cement and Concrete Research*, 76, 130-146.

Rao, M., and Lakshmi, K. P. (2005). "Analysis of b-value and improved b-value of acoustic emissions accompanying rock fracture." *Current science*, 1577-1582.

Sagasta, F., Benavent-Climent, A., Fernández-Quirante, T., and Gallego, A. (2014). "Modified Gutenberg–Richter coefficient for damage evaluation in reinforced concrete structures subjected to seismic simulations on a shaking table." *Journal of Nondestructive Evaluation*, 33(4), 616-631.

Sagasta, F. A., Torné, J. L., Sánchez-Parejo, A., and Gallego, A. (2013). "Discrimination of acoustic emission signals for damage assessment in a reinforced concrete slab subjected to seismic simulations." *Archives of Acoustics*, 303-310.

Saouma, V., and Perotti, L. J. A. m. j. (2006). "Constitutive model for alkali-aggregate reactions." 103(3), 194.

Saouma, V. E., and Hariri-Ardebili, M. A. (2014). "A proposed aging management program for alkali silica reactions in a nuclear power plant." *Nuclear Engineering Design*, 277, 248-264.

Sauerbrunn, C. M. (2016). "Evaluation of information entropy from acoustic emission waveforms as a fatigue damage metric for Al7075-T6." Master of Science, University of Maryland.

Shannon, C. E. (1948). "A mathematical theory of communication." *The Bell system technical journal*, 27(3), 379-423.

Shin, H.-C., Orton, M. R., Collins, D. J., Doran, S. J., and Leach, M. O. (2012). "Stacked autoencoders for unsupervised feature learning and multiple organ detection in a pilot study using 4D patient data." *IEEE transactions on pattern analysis machine intelligence*, 35(8), 1930-1943.

Shiotani, T. (1994). "Evaluation of progressive failure using AE sources and improved b-value on slope model tests." *Progress in Acoustic Emission VII*, 529-534.

Shiotani, T., Nishida, T., Nakayama, H., Asaue, H., Chang, K.-C., Miyagawa, T., and Kobayashi, Y. (2017). "Fatigue Failure Evaluation of RC Bridge Deck in Wheel Loading Test by AE Tomography." *Advances in Acoustic Emission Technology*, Springer, 251-264.

Solomatine, D., See, L. M., and Abrahart, R. (2009). "Data-driven modelling: concepts, approaches and experiences." *Practical hydroinformatics*, Springer, 17-30.

Soltangharaei, V. (2020). "Evaluation of Temporal Damage Progression in Concrete Structures Affected by ASR Using Data-driven Methods." Doctoral dissertation, University of south carolina.

Soltangharaei, V., Ai, L., Anay, R., Bayat, M., and Ziehl, P. (2021a). "Implementation of Information Entropy, b-Value, and Regression Analyses for Temporal Evaluation of Acoustic Emission Data Recorded during ASR Cracking." *Practice Periodical on Structural Design Construction*, 26(1), 04020065.

Soltangharaei, V., Anay, R., Ai, L., Giannini, E. R., Zhu, J., and Ziehl, P. (2020a). "Temporal Evaluation of ASR Cracking in Concrete Specimens Using Acoustic Emission." *Journal of Materials in Civil Engineering*, 32(10), 04020285.

Soltangharaei, V., Anay, R., Assi, L., Bayat, M., Rose, J., and Ziehl, P. (2021b). "Analyzing acoustic emission data to identify cracking modes in cement paste using an artificial neural network." *Construction Building Materials*, 267, 121047.

Soltangharaei, V., Anay, R., Begrajka, D., Bijman, M., ElBatanouny, M., Ziehl, P., and Van Tooren, M. J. (2019a). "An Impact Event Detection System for Composite Box Structures." *COMADEM 2019*Huddersfield, United Kingdom.

Soltangharaei, V., Anay, R., Begrajka, D., Bijman, M., ElBatanouny, M. K., Ziehl, P., and Van Tooren, M. J. "A minimally invasive impact event detection system for aircraft movables." *Proc., AIAA Scitech 2019 Forum*, 1268.

Soltangharaei, V., Anay, R., Begrajka, D., Bijman, M., ElBatanouny, M. K., Ziehl, P., and van Tooren, M. J. (2020b). "An Impact Event Detection System for Composite Box Structures." *Advances in Asset Management and Condition Monitoring*, Springer, Advances in Asset Management and Condition Monitoring, 1063-1073.

Soltangharaei, V., Anay, R., Hayes, N., Assi, L., Le Pape, Y., Ma, Z., and Ziehl, P. (2018). "Damage mechanism evaluation of large-scale concrete structures affected by alkali-silica reaction using acoustic emission." *Applied Sciences*, 8(11), 2148.

Soltangharaei, V., Hill, J., Ai, L., Anay, R., Greer, B., Bayat, M., and Ziehl, P. (2020c). "Acoustic emission technique to identify stress corrosion cracking damage." *Structural Engineering Mechanics*, 75(6), 723-736.

Sun, Y., Zhang, H., Zhao, T., Zou, Z., Shen, B., and Yang, L. (2020). "A New Convolutional Neural Network With Random Forest Method for Hydrogen Sensor Fault Diagnosis." *IEEE Access*, 8, 85421-85430.

Suzuki, H., Kinjo, T., Hayashi, Y., Takemoto, M., Ono, K., and Hayashi, Y. (1996a). "Wavelet transform of acoustic emission signals." *Journal of acoustic emission*, 14, 69-84.

Suzuki, H., Kinjo, T., Hayashi, Y., Takemoto, M., Ono, K., and Hayashi, Y. (1996b). "Wavelet transform of acoustic emission signals." *Journal of Acoustic Emission*, 14, 69-84.

Szegedy, C., Liu, W., Jia, Y., Sermanet, P., Reed, S., Anguelov, D., Erhan, D., Vanhoucke, V., and Rabinovich, A. "Going deeper with convolutions." *Proc., Proceedings of the IEEE conference on computer vision and pattern recognition*, 1-9.

Szegedy, C., Vanhoucke, V., Ioffe, S., Shlens, J., and Wojna, Z. "Rethinking the inception architecture for computer vision." *Proc., Proceedings of the IEEE conference on computer vision and pattern recognition*, 2818-2826.

Tan, P. N., Steinbach, M., and Kumar, V. (2013). "Data mining cluster analysis: basic concepts and algorithms." *Introduction to data mining*.

Tan, P. N., Steinbach, M., and Kumar, V. (2018). "Data mining cluster analysis: basic concepts and algorithms." *Introduction to data mining*, Pearson Education, New York, NY, USA.

Villeneuve, V., Fournier, B., and Duchesne, J. "Determination of the Damage in Concrete Affected by ASR—the Damage rating Index (DRI)." *Proc., 14th International Conference on Alkali-Aggregate Reaction (ICAAR). Austin, Texas (USA)*.

Wang, J.-G., Wang, Y., Yao, Y., Yang, B.-H., and Ma, S.-W. (2019). "Stacked autoencoder for operation prediction of coke dry quenching process." *Control Engineering Practice*, 88, 110-118.

Ziehl, P., and ElBatanouny, M. (2015). "Low-level acoustic emission in the long-term monitoring of concrete." *Acoustic Emission and Related Non-Destructive Evaluation Techniques in the Fracture Mechanics of Concrete*, Elsevier, 205-224.